Green Chemistry

PAPER

View Article Online
View Journal | View Issue

Cite this: *Green Chem.*, 2023, **25**, 8241

Feedstock agnostic upcycling of industrial mixed plastic from shredder residue pragmatically through a composite approach†

Kanjanawadee Singkronart, [a] Andre Gaduan, [a] Siti Rosminah Shamsuddin,[a] Keeran Ward [c] and Koon-Yang Lee *[a,b]

Shredding of a vehicle or an electrical and electronic equipment at its end-of-life (EOL) is a common practice to extract valuable critical raw materials. Unfortunately, this has the unintended consequence of mixing different polymers together and the only EOL options for this industrial mixed plastic waste are landfilling and incineration. Here in this work, we show that low value and highly heterogenous industrial mixed plastic can be mechanically upcycled sustainably using a composite approach, *i.e.*, reinforcing with carbon fibres (CFs), glass fibres (GFs) and wood flour (WF). It was found that industrial mixed plastic can be successfully reprocessed, albeit possessing significantly poorer mechanical properties compared to its virgin counterpart. Nevertheless, the mechanical properties of the reinforced industrial mixed plastics were observed to be governed by the fibre or filler reinforcement, instead of the more inferior brittle industrial mixed plastic matrix. A lifecycle analysis (LCA) model with a functional unit designed using finite element analysis was developed to determine the environmental impact of upcycling industrial mixed plastic from shredder residue using this composite approach. In a "business as usual" scenario, our LCA model estimated a global warming potential (GWP) of 23 kg CO_2-eq. per f.u. and a net abiotic depletion potential of fossil (ADPf) of 431 MJ f.u.$^{-1}$. Using our proposed feedstock agnostic and pragmatic solution, the GWP and net ADPf could be reduced to only 11 kg CO_2-eq. per f.u. and 160 MJ f.u.$^{-1}$, respectively, when 40 wt% WF reinforcing filler was used. Our work also reports the influence of reinforcement on the tensile, flexural and fracture toughness properties, as well as the LCA hot spots in such an upcycling approach.

Received 19th June 2023,
Accepted 30th August 2023

DOI: 10.1039/d3gc02198j

rsc.li/greenchem

1. Introduction

Increasing disposable income, growing urbanisation and mobility are fuelling the growth of the automotive and the electrical and electronic equipment (EEE) sectors. The global EEE sector grew to US$3.5 trillion in 2022, with a compound annual growth rate (CAGR) of 6.5%.[1] Even though the COVID-19 pandemic severely disrupted the supply chain of the automotive sector, there are signs of recovery with a 3% increase in global motor vehicle production between 2020 and 2021.[2] Associated with these growths, however, are the increase in the demand for engineering plastics. In Europe alone, the engineering plastics demand in the automotive and EEE sectors has grown from 7.2 million tonnes in 2015 to 8.1 million tonnes in 2019[3,4] and is anticipated to reach 11 million tonnes by the year 2030.[5] At the end-of-life of a vehicle or an electrical/electronic equipment, it is first disassembled to retain any reusable parts and batteries.[6–8] After which, it is shredded to further extract the more valuable critical raw materials, such as ferrous and non-ferrous metals. The process of shredding also leads to an unintended consequence of mixing different types of engineering plastics together. Consequently, the sorting of this mixed plastic from the shredder residue, which often includes acrylonitrile-butadiene-styrene (ABS), polystyrene (PS), polypropylene (PP), polyethylene (PE) and thermosets,[3,4,7,8] is difficult to achieve due the overlapping densities and conductivities. Moreover, these plastics are often not labelled, which make polymer identification a challenge. As a result, industrial mixed plastic from shredder residue is typically sent to landfill or is incinerated.[6,9]

An easy solution to reduce the environmental impact of industrial mixed plastic is to recover and reprocess it into new products. However, these products will possess inferior mechanical performance compared to their virgin counter-

[a]*Department of Aeronautics, Imperial College London, South Kensington Campus, London, SW7 2AZ, UK. E-mail: koonyang.lee@imperial.ac.uk*
[b]*Institute for Molecular Science and Engineering (IMSE), Imperial College London, London, SW7 2AZ, UK*
[c]*School of Chemical and Process Engineering, University of Leeds, Lees, LS2 9JT, UK*
† Electronic supplementary information (ESI) available. See DOI: https://doi.org/10.1039/d3gc02198j

parts. For example, ABS and polycarbonate (PC) possess a tensile strength of 40 MPa and 55 MPa, respectively. The blending of ABS and PC, however, produces a polymer blend with a tensile strength as low as 31 MPa.[10] More importantly, an ABS/PC blend possesses low work-of-fracture due to its low strain-at-failure (2%) compared to virgin ABS (51%) and PC (8%). Similar findings have also been observed for many engineering polymer blends, including ABS/PS,[11] PS/PP,[12] ABS/PA,[13] PC/PS,[13] PC/PP,[14] PMMA/PS[14] and ABS/PET.[15] This is because most polymers are not miscible at the molecular level (*i.e.*, the Gibbs free energy of polymers mixing, $\Delta G^{mix} > 0$). To address this challenge, compatibilisers can be employed.[16–23] Compatibilisers work by lowering the interfacial tension between the immiscible polymers, stabilising the dispersed phase against coalescence and improving the adhesion between the different polymer phases. One must note that compatibilisers are not feedstock agnostic[18–23] as they are designed for specific binary polymer combinations.[16,17] It is already a challenge to predict the exact composition of any stream in a polymer recycling process, let alone the residue after shredding of different automotive and electrical/electronic parts together. This makes the selection of a suitable compatibiliser for a batch of industrial mixed plastic difficult.

In a previous work, we have reported a feedstock agnostic approach of using high performance carbon fibres (CFs) to upgrade the mechanical performance of immiscible PP/PET binary blend.[24] The mechanical performance of the model CF-reinforced PP/PET composite blend is dominated by the stronger reinforcing CFs instead of the inferior immiscible PP/PET matrix. This mechanical upcycling method allowed us to broaden the application of immiscible PP/PET binary blends for various higher value end-uses. Here in this work, we expand our feedstock agnostic and pragmatic upcycling concept to industrial mixed plastic from the shredding of end-of-life vehicle and waste electrical and electronic equipment (see Fig. 1a). Three types of reinforcements, namely wood flour (WF), glass fibres (GFs) and CFs, are investigated. This present work focuses on the challenge associated with the identification of a suitable processing window to melt industrial mixed plastic from shredder residue, the fabrication of reinforced industrial mixed plastics and discusses the effect of different reinforcements on their mechanical response. Results from life-cycle assessment (LCA) is also reported to quantify the environmental impact associated with the use of different reinforcements to upcycle industrial mixed plastic from shredder residue.

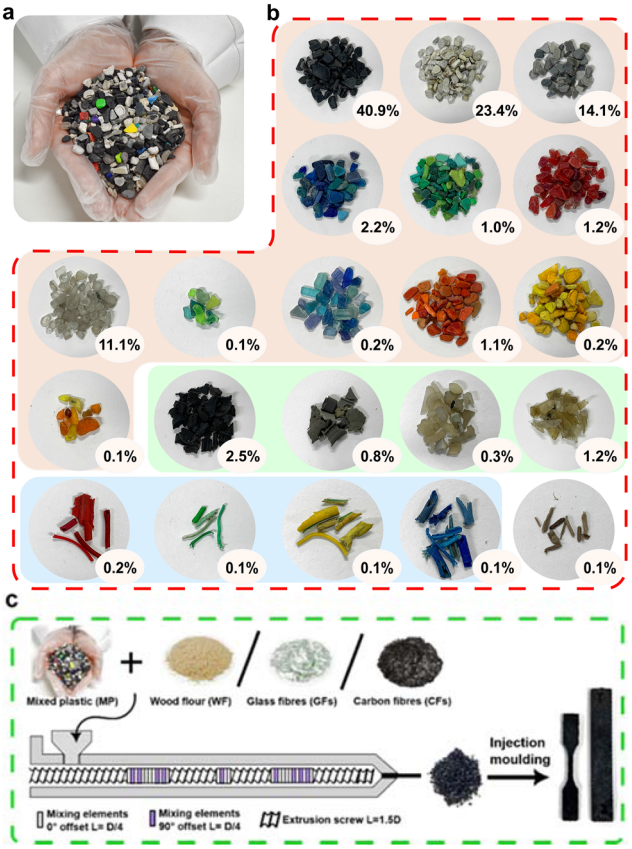

Fig. 1 (a) As received industrial mixed plastic from the shredding of end-of-life vehicle and WEEE plastics, which was then (b) hand sorted based on colour and rigidity. Granules in the red, green and blue shaded regions of the figure are "rigid" plastics, "non-rigid" rubber and "non-rigid" insulation wire, respectively. Wood fragments (in the unshaded region) were also found in our batch of industrial residual mixed plastic. (c) Schematic summarising the manufacturing of fibre- and filler-reinforced industrial residual mixed plastics.

2. Materials and methods

2.1 Materials

Industrial mixed plastic from shredder residue was kindly supplied by Axion Polymers (Manchester, UK). Based on the data provided, this batch of mixed plastic (see Fig. 1a) composed of 40–50 wt% ABS, 30–40 wt% PS, 10–15 wt% PP, 3 wt% rubber, 2 wt% PE and the remainders are unidentifiable. Sized chopped intermediate modulus CF tows (Carbiso CT IM56D, diameter = 7 μm, length = 6 mm) were purchased from ELG Carbon Fibre Ltd (Coseley, UK). Sized chopped E-glass fibres (E-562A, diameter = 13 μm, length = 6 mm) were purchased from Jushi Group co. Ltd (Wutong District, Tongxiang, Zhejiang, CN). WF (EPC200, mesh size = 180) was purchased from Eden Products Ltd (Middlewich, UK) and dried at 80 °C for 2 hours prior to subsequent use.

2.2 Fabrication of reinforced industrial mixed plastics

A schematic diagram summarising the fabrication of fibre- and filler-reinforced industrial mixed plastics is presented in Fig. 1c. All samples were compounded using a co-rotating twin-screw extruder (Eurolab XL, Thermo Fischer Scientific, Karlsruhe, Germany) equipped with two 16 mm diameter screws. The length-to-diameter ratio of the screws is 25 and a screw speed of 30 rpm was used. The screw profile can be found in Gaduan *et al.*[64] A processing temperature of 210 °C was selected in this work based on a parametric study conducted (see sections 3.1 and 3.2 later). Prior to compounding,

the mixed plastic granules and the reinforcing fibres (GFs, CFs) or fillers (WF) were dry-mixed manually in batches of 500 g at the different loadings (2.5 wt%, 5 wt%, 10 wt%, 20 wt% and 40 wt%). After compounding, the extrudate was pelletised (Haake VariCut, Thermo Fischer Scientific, Karlsruhe, Germany) into 3 mm long pellets and injection moulded (Haake Minijet Pro Thermo Fischer Scientific, Karlsruhe, Germany) into dog bone-shaped and rectangular test specimens. The barrel and mould temperatures of the injection moulder were set to 210 °C and 40 °C, respectively. All specimens were injection moulded at an injection pressure of 65 MPa for 10 s, followed by a holding pressure of 65 MPa for 60 s. The dog bone test specimen possessed an overall length of 65 mm, a thickness of 3 mm, a gauge length of 10 mm and the narrowest part of the dog bone specimen was also 3 mm. The rectangular test specimen possessed an overall length of 80 mm, a width of 13 mm and a thickness of 3 mm. Unreinforced mixed plastic granules were also extruded and injection moulded using the same processing steps.

2.3 Material characterisations

2.3.1 Thermal stability of the different mixed plastic granules. The thermal degradation behaviour of the industrial mixed plastic was investigated using thermal gravimetric analysis (TGA) (Q500, TA Instruments, Newcastle, UK). Prior to the measurement, the different mixed plastic granules were manually sorted based on colour and rigidity (see Fig. 1b). A sample mass of ~12 mg was heated from room temperature to 600 °C at a rate of 10 °C min^{-1} in air.

2.3.2 Differential scanning calorimetry (DSC) study of the different mixed plastic granules. DSC (Discovery DSC, TA Instruments, Hertfordshire, UK) was used to identify a suitable processing temperature for this industrial mixed plastic. Similar to the TGA measurement, DSC was also conducted for each type of granule based on colour and rigidity. A sample mass of 10 mg was used. This measurement was conducted in an N_2 atmosphere and the sample was heated from −10 to 300 °C at a rate of 10 °C min^{-1}.

2.3.3 Porosity of (reinforced) mixed plastics. The true density (ρ_{true}) of the industrial mixed plastic, as well as the GFs, CFs and WF used in this work was measured using He pycnometery (Accupyc II 1340, Micrometrics Ltd, Dunstable, UK). The envelope density (ρ_E) of the injection moulded (reinforced) mixed plastics was determined from the ratio between the mass and the envelope volume of the sample. The porosity (P) of the samples was then calculated using

$$P, \% = \left(1 - \frac{\rho_E}{\rho_{true}}\right) \times 100 \quad (1)$$

2.3.4 Mechanical properties of (reinforced) mixed plastics. Tensile, flexural (3-point bending) and fracture toughness properties of the (reinforced) mixed plastics were investigated in accordance with ASTM D638-14, ASTM D790-17 and ASTM5045-14, respectively. These tests were conducted using an Instron universal tester (Model 5960, Instron Corporation, High Wycombe, UK) equipped with a 10 kN load cell. A total of five specimens were tested for each type of sample in each test. Prior to tensile testing, two dots were marked on the surface of the dog bone-shaped tensile test specimen in the direction of applied load. The strain experienced by the test specimen under uniaxial tensile loading was then evaluated by monitoring the movement of these two dots using a non-contact optical extensometer (IMT-CAM027, iMetrum Ltd, Bristol, UK). A crosshead displacement speed of 1 mm min^{-1}, which corresponded to a strain rate of 0.1% s^{-1}, was used. Flexural test was conducted in 3-point bending mode using a crosshead displacement speed of 1 mm min^{-1}. A span length of 55 mm was used (corresponded to a span-to-thickness ratio of 16). To accurately track the bending of the rectangular flexural test specimen, the displacement of the loading nose was tracked using a camera (IMT-CAM027, iMetrum Ltd, Bristol, UK). The fracture toughness of the (reinforced) mixed plastics was determined from single-edge notch beam (SENB) test specimens. Prior to this test, a sharp notch with a depth of 6.2 mm was introduced at the halfway point lengthwise using a band saw (Startrite 502S, A.L.T. Saws & Spares Ltd, Kent, UK) and further sharpened with a surgical scalpel. The initial crack length (a) to width (w) ratio, x, was ~0.49. The SENB test specimen was then loaded under three-point bending (50 mm support span length) using a crosshead displacement speed of 1 mm min^{-1}. The initial critical stress intensity factor, K_{IC}, of specimen was calculated from

$$K_{IC}, \mathrm{MPa\,m^{0.5}} = \left(\frac{P}{bw^{0.5}}\right) \times 6\sqrt{x}\left(\frac{1.99 - x(1-x)(2.15 - 3.93 + 2.7x^2)}{(1+2x)(1-x)^{1.5}}\right) \quad (2)$$

where P is the load at crack initiation and b is the thickness of the test specimen.

2.3.5 Structure and morphology of (reinforced) mixed plastics. Scanning electron microscopy (SEM) (S-3700N, Hitachi High-Technologies Corporation, Tokyo, Japan) was conducted using an accelerating voltage of 10 kV. Prior to SEM, the samples were mounted onto aluminium stubs using carbon tabs. It was then Au coated (Agar Auto Sputter coater, Agar Scientific Ltd, UK) using a coating current of 40 mA for 20 s.

2.3.6 Lifecycle assessment (LCA). LCA can provide a comprehensive analysis of the environmental impact of a product or service.[25] In this work, LCA was conducted to evaluate whether the addition of WF, GFs and CFs could be used to upgrade industrial mixed plastic *sustainably*. The goal of this LCA is to quantify the environmental impact of the (reinforced) mixed plastics through a cradle-to-grave assessment that includes raw materials production, (re)processing, use and disposal. The functional unit (f.u.) of our LCA model was chosen as the equivalent mass of (reinforced) mixed plastic that is required to achieve the same mechanical performance as a chair made from virgin PP. Three different life-cycle scenarios were considered in our LCA model and the system boundary is

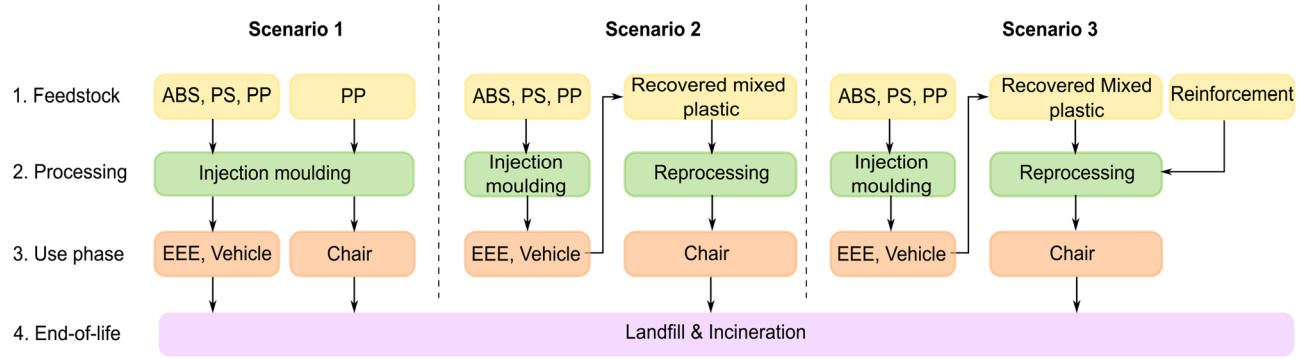

Fig. 2 Schematic diagram showing the three scenarios modelled in our LCA.

shown schematically in Fig. 2. Industrial mixed plastic was modelled as 50% ABS, 40% PS and 10% PP in our LCA model. Scenario 1 corresponds to "business as usual", whereby virgin ABS, PS and PP are produced and disposed of at its end-of-life whilst additional virgin PP are produced and used to manufacture a chair, which is also disposed of at its end-of-life. In scenario 2, virgin ABS, PS and PP are still manufactured and recovered as industrial mixed plastic to be reprocessed into a chair. Consequently, the production of additional virgin PP for the chair is avoided. Scenario 3 is an extension of scenario 2, whereby the reinforcing CFs, GFs and WF are produced and added to the industrial mixed plastic to manufacture a chair made out of reinforced mixed plastic. Our LCA model further assumes that 20% of the PP chairs produced would go to landfill and 80% would be incinerated (in the presence of O_2) for energy recovery, whilst 50% of the industrial mixed plastic would go to landfill and the remaining 50% would be incinerated for energy recovery. These percentages are based on the current end-of-life practices in the UK.[9] In addition, we also modelled the steam gasification (in the absence of O_2) of the industrial mixed plastic from shredder residue as a pathway to cleaner power generation, whereby thermal energy is transformed to electrical energy utilising thermodynamic cycles. This is also a practice that has been employed in Japan[26] and the US.[27] This gasification process for energy recovery was modelled using Aspen Plus and the details of this process can be found in ESI S1.†

To obtain the mass of the f.u. in each scenario, finite element analysis was used (Abaqus 2019, Dassault Systèmes Simulia Corp.). A finite element model of the chair was constructed using 199 317 quad shell elements containing four nodes each (type S4R) and modelled using the Abaqus/Standard module. The mesh convergence study can be found in ESI S2.† The material was treated as an elastic isotropic solid with 4 fixed points (encastré) that corresponded to the 4 legs of the chair (not simulated). The body pressure applied on the chair was simulated based on the physical attributes[28] of a typical 25 years old man with a height of 1.70 m and a body weight of 65 kg (see Fig. 3).

Our LCA model used the CML 2001 impact assessment method (January 2016 version) and was conducted using the

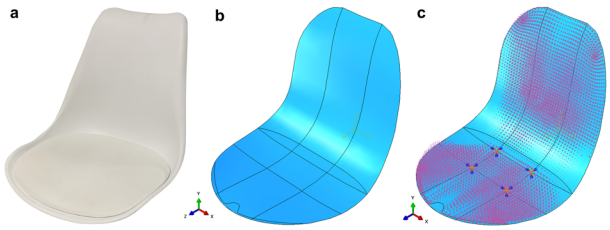

Fig. 3 (a) A chair as the functional unit in our LCA model (b) virtually and (c) with a map showing the pressure distribution of a man sitting on it.[28]

lifecycle engineering software, GaBi (version 9, Sphera Solutions GmbH). The chosen impact categories in our LCA model were global warming potential (GWP) and abiotic depletion of fossil potential (ADPf). All data used in our LCA model were obtained from (i) the GaBi Professional database (version 9, Sphera Solutions GmbH, Leinfelden-Echterdingen, Germany), (ii) the literature and (iii) our own estimations. A detailed inventory is included (see ESI S3†). Electricity usage was modelled based on a typical Great Britain electricity mix. The energy requirement to produce the f.u. (ΔE) is calculated using

$$\Delta E = m_{\text{f.u.}}\left[\int_{25}^{T} C_{\text{p, f.u.}}\,\mathrm{d}T + \Delta H_{\text{m}}\right]\left(1 + \frac{T-25}{25}\right) \quad (3)$$

where $C_{\text{p,f.u.}}$, $m_{\text{f.u.}}$ and ΔH_{m} denote the specific heat capacity, mass and specific heat of fusion of the f.u., respectively. The processing temperature used, T, was 190 °C for the production of the PP chair and 210 °C for the processing of the (reinforced) industrial mixed plastics. The environmental impact associated with CFs production was obtained from the cradle-to-gate LCA model developed by Meng *et al.*[29] for the manufacturing of polyacrylonitrile (PAN) based CFs. The production of WF in our LCA considered the forestation of spruce and the grinding of wood logs into fine particles.[30] The energy requirement for the recycling of industrial mixed plastic was modelled based on the LCA model developed by Ciacci *et al.*[31] The environmental impact associated with the transportation of materials was not considered.

3. Results and discussion

3.1 Thermal behaviour of the different mixed plastic granules

One of the main challenges in the re-processing of mixed plastic is the mismatch in the melting temperature of the different polymers.[32] On one hand, selecting a processing temperature for a mixed plastic based on the polymer with the highest melting temperature may cause thermal degradation to those with a lower melting temperature. On the other hand, using a processing temperature based on the polymer with the lowest melting temperature may lead to poor flowability and consolidation of the mixed plastic. In addition to this, commercial polymer formulations may contain up to 70 wt% additives, including colour pigments, lubricating agent, antioxidant and others.[33–37] Selecting the wrong processing temperature may cause the degradation of these additives, forming voids within the melt consolidated mixed plastic. The degradation product of a polymer could also cause hydrolysis of another polymer in the same batch.[38]

We therefore first investigated the thermal properties of the different mixed plastic granules individually. As aforementioned, the as-received industrial mixed plastic was manually sorted into 21 different types of granules based on colour and rigidity (see Fig. 1b). The major constituent in this industrial mixed plastic was found to be rigid polymers, which made up *ca.* 94 wt% (highlighted in red). The remainders were the non-rigid rubber (*ca.* 5 wt%, highlighted in green) and non-rigid polymers used for wire insulation (*ca.* 0.4 wt%, highlighted in blue). To our surprise, we also found wood fragments mixed into this batch of industrial mixed plastic. Fig. 4a and b present the thermal stability of the different mixed plastic granules in air. A variety of thermal degradation behaviour can be observed for both the rigid (Fig. 4a) and non-rigid (Fig. 4b) fractions. Whilst it is impossible to correlate the different thermal degradation behaviour to a specific polymer, it did provide us with an upper processing temperature limit. Based on the results obtained, the processing temperature of this industrial mixed plastic should not exceed 250 °C.

Given this upper temperature limit, DSC was further conducted to identify a suitable melt processing window. It was found that the rigid fraction is made of thermoplastics (see Fig. 4c). Granules that exhibited a melting temperature of 165 °C correspond to PP, based on the given materials data. To our surprise, some granules (~5 wt%) were found to possess a melting temperature of 225 °C and 240 °C, which could correspond to PA and PET, respectively. This is not highlighted in the data sheet, further signifying the challenge in using industrial mixed plastic from shredder residue as feedstock due to difficulties in obtaining exact composition. The amorphous thermoplastics in the rigid fraction were found to possess glass transition temperatures of 100 °C and 145 °C, which correspond to ABS and PS, as well as possibly PC, respectively. No observable melting temperature was observed for the non-rigid fraction (see Fig. 4d). Instead, the observed exotherm at temperature >230 °C can be attributed to vulcanisation reaction[39,40] while the endotherm at temperature >250 °C corroborates with the thermal degradation of rubber.[40] It follows that the processing window for this industrial mixed plastic should be between 170 and 230 °C.

3.2 Tensile properties of the industrial mixed plastic melt-processed at different temperatures

Fig. 4e presents the tensile properties of the industrial mixed plastic melt-processed and injection moulded at different temperatures, namely 170 °C, 190 °C, 210 °C and 230 °C. All tensile test specimens possessed a porosity of ~1%, implying that these melt-processing temperatures did not lead to the volatilisation of any polymer additives that may be present. The tensile modulus (green curve), tensile strength (red curve) and tensile strain-at-break (blue curve) were found to increase with increasing processing temperature before plateauing at a processing temperature of 210 °C. The poorer tensile properties at lower processing temperatures (*i.e.*, 170 °C and 190 °C) can be attributed to poor melt consolidation as these processing temperatures were not high enough to melt some of the rigid polymers in the industrial mixed plastic. By correlating the DSC thermogram with the composition of each type of mixed plastic granules, we identified more than 5 wt% mixed plastic granules that possesses a melting point greater than 190 °C. The non-melted mixed plastic granules created defects within the material, leading to earlier onset failure. As a further increase in processing temperature to 230 °C did not lead to an increase in tensile properties, a processing temperature of 210 °C was chosen for subsequent composite processing.

Industrial mixed plastic injection moulded at this temperature possessed a tensile modulus, tensile strength and strain-at-break of 2.9 GPa, 32 MPa and 1.5%, respectively. As a benchmark for comparison, we also measured the tensile properties of virgin ABS, PP, PS and HDPE. Virgin ABS possesses a tensile modulus of 2.0 GPa, tensile strength of 42 MPa and strain-at-break of 77%. Virgin PP and PS possess a tensile modulus of 1.8 GPa and 3.7 GPa, respectively, a tensile strength of 32 MPa and 57 MPa, respectively, as well as a strain-at-break of 4.8% and 578%, respectively. The tensile modulus, tensile strength and strain-at-failure of HDPE were 1.2 GPa, 20 MPa and 416%, respectively. The inferior tensile strength and strain-at-failure of the injection moulded industrial mixed plastic can be attributed to the immiscibility between the different polymers as they possess very different solubility parameter (δ) values (δ_{ABS}: 21.0 (J cm^{-3})$^{0.5}$, δ_{PS}: 19.5 (J cm^{-3})$^{0.5}$, δ_{PP}: 15.2 (J cm^{-3})$^{0.5}$ and δ_{PE}: 16.4 (J cm^{-3})$^{0.5}$).[17] In a typical immiscible binary blend such as PS-PP and PP-PET, either a sea-island or co-continuous microstructure is formed depending on the relative fraction of the two phases.[12,17,24] Such heterogenous microstructures act as stress concentration points, deteriorating the mechanical performance of the resulting immiscible binary blend. The internal morphology of the injection moulded industrial mixed plastic is shown in Fig. 5. Due to its multi-component nature, a sea-island microstructure (Fig. 5a) along with distinct

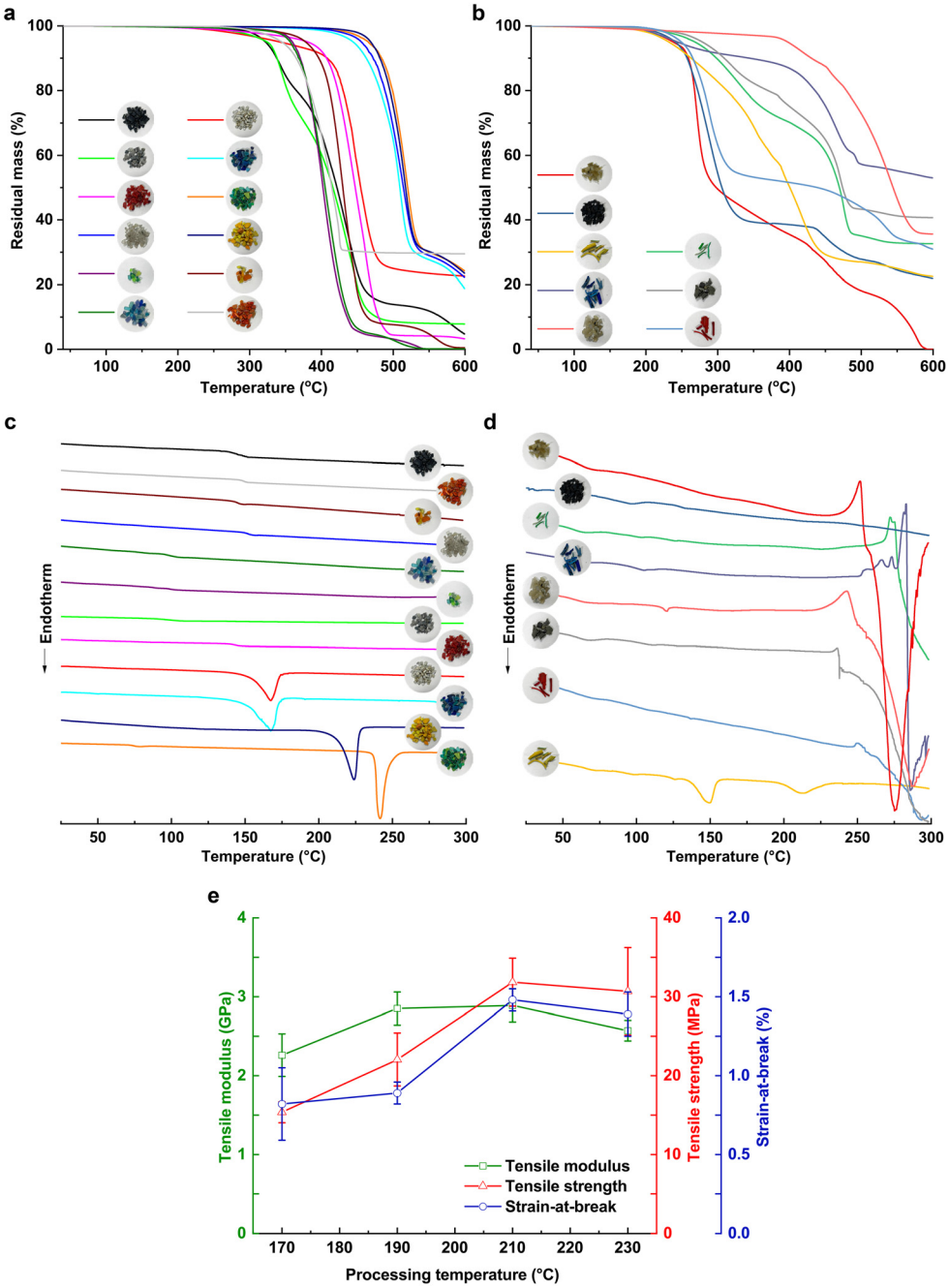

Fig. 4 Thermal and mechanical properties of industrial mixed plastic. Thermal stability in air (a, b) and DSC thermograms (c, d) of the "rigid" and "non-rigid" fractions of the industrial residual mixed plastic granules, respectively. (e) Tensile properties of the injection moulded industrial mixed plastic as a function of processing temperature.

polymer domains (Fig. 5b) co-exist together. These micro-voids and polymer inclusion could act as a precursor which lead to brittle failure.[10,41] With inconsistent shapes and sizes of the sea-island morphology, this may initiate multiple fracture sites leading to multiple crack planes (Fig. 5b and c). Moreover, the injection moulded mixed plastic also contained rubber, which cannot be melted due to its cross-linked nature and could also contribute to premature failure.

3.3 Tensile and flexural properties of model reinforced mixed plastics

The tensile and flexural properties of CF-reinforced (red curve), GF-reinforced (blue curve) and WF-filled (green curve) mixed plastics are presented in Fig. 6. It can be seen from this figure that CFs, GFs and WF were able to reinforce the brittle mixed plastic matrix. The tensile (Fig. 6a) and flexural (Fig. 6b)

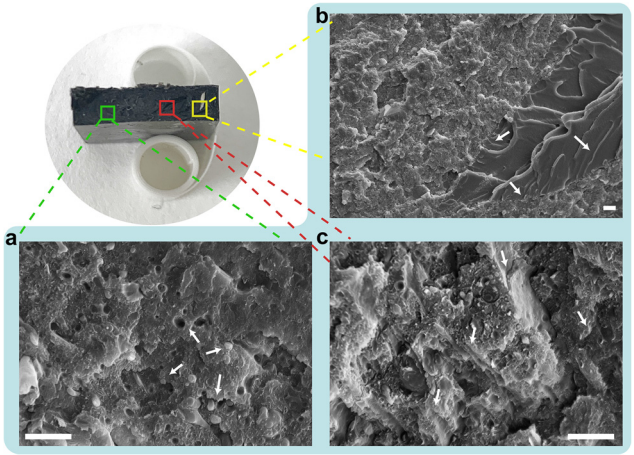

Fig. 5 SEM images of the cryo-fractured surface of injection moulded industrial mixed plastic. Scale bar = 5 μm.

modulus of the model CF- and GF-reinforced, as well as WF-filled mixed plastics increased monotonically with increasing loading. At a loading of 40 wt%, the resulting composites achieved 22 GPa and 17 GPa, for CF-reinforced, 13 GPa and 9 GPa for GF-reinforced, as well as 7.5 GPa and 6.5 GPa for WF-filled mixed plastics in tension and bending, respectively. In a fibre-reinforced composite system, the elastic modulus is the weighted average of the elastic modulus of the reinforcement and the polymer matrix, respectively.[42] Since both CFs and GFs possess higher tensile modulus than the brittle mixed plastic matrix, the modulus of the resulting CF- and GF-reinforced mixed plastics increased as expected. The relative elastic modulus of a particulate-filled polymer (*i.e.*, the ratio between the elastic modulus of the filled and unfilled polymer) is an increasing function that depends on the filler content and filler size.[43] Consequently, the modulus of WF-filled mixed plastic increases with increasing WF loading.

The tensile (Fig. 6c) and flexural (Fig. 6d) strength of the model CF- and GF-reinforced mixed plastics were also found to increase monotonically with the loading of reinforcing fibres. At 40 wt% loading, model CF- and GF-reinforced mixed plastics achieved a tensile strength of 67 MPa and 51 MPa, respectively; 110% and 60% improvement over unreinforced mixed plastic. The flexural strength of CF- and GF-reinforced mixed plastics increased by 120% and 33% over unreinforced mixed plastic at the same fibre loading. This can be attributed to the good compatibility between the reinforcing CFs and GFs with ABS and PS (see section 3.4 later), which are the two major polymer matrices in the mixed plastic system. The incorporation of WF into the industrial mixed plastic matrix however, had a detrimental effect both the tensile and flexural strength up to 10 wt% WF. The tensile strength of the model WF-filled mixed plastic decreased by 10% to ~28 MPa compared to unfilled mixed plastic before increasing to 40 MPa at 40 wt% loading (see Fig. 6b, green curve). Similarly, the flexural strength of the model WF-filled mixed plastic decreased by 10% to 43 MPa before increasing to 57 MPa when the WF loading increased to 40 wt%. If good compatibility exists between WF and the polymer matrix, the strength of the resulting WF-filled polymer is expected to increase with increasing filler content.[44] Conversely, if the compatibility between WF and the polymer matrix is poor, the strength of the WF-filled polymer should decrease with increasing filler content. However, a minimum in strength was observed. This is thought to be due to (i) the selective dispersion of WF in a particular polymer phase at low filler content and (ii) the bridging of the phase boundaries between different immiscible polymers at high filler content. The decrease in tensile and flexural strength can be attributed to the former and the increase in tensile and flexural strengths could be attributed to the latter.

3.4 SENB fracture toughness of model reinforced mixed plastics

Fig. 6e summarises the SENB K_{IC} of the mixed plastic reinforced with CFs and GFs, as well as filled with WF. Unreinforced mixed plastic was found to possess a low K_{IC} of 0.94 MPa $m^{0.5}$. Such low fracture resistance can be attributed to the heterogeneous microstructure of unreinforced mixed plastic (see Fig. 5). The addition of CFs, GFs and WF improved the fracture toughness of the resulting mixed plastic composites as the introduction of reinforcement in the form both fibres and fillers created additional energy absorbing mechanisms during crack propagation, such as crack diversion, fibre/filler-matrix debonding, pull out and fracture.[42] It can also be seen that the fracture toughness of all the mixed plastic composites increased by the same extent up to 5 wt% loading. A further increase in the loading of GFs and WF did not lead to an increase in the K_{IC} of GF-reinforced and WF-filled mixed plastics. The K_{IC} of these mixed plastic composites plateaued at 1.5 MPa $m^{0.5}$. With CFs as the reinforcement, the K_{IC} of the resulting composites increased further with increasing CF loading up to 20 wt% before a plateau at 2.7 MPa $m^{0.5}$. To further elucidate the reason behind the higher SENB K_{IC} plateau of CF-reinforced mixed plastic compared to its GF-reinforced and WF-filled counterparts, fractographic analysis was further conducted.

Unreinforced mixed plastic exhibited textured microflow (Fig. 7a, label 1), riverline (Fig. 7a, label 2) and a distinct lack of plastic deformation, which are characteristics of a brittle material. Non-melted polymer inclusion was also observed (Fig. 7a, label 3). The SENB fracture surface of WF-filled mixed plastic (Fig. 7b) showed a rough texture and significant fibrillation, implying that the main mechanism behind the improvement in SENB fracture toughness response is due to the fibrillation of wood fibre and voids nucleation developing at the interface between the brittle mixed plastic matrix and the reinforcing WF filler. Fig. 7c and d present the mode I fracture surfaces of GF-reinforced and CF-reinforced mixed plastics, respectively. In general, the fracture of short fibre composites can be classified into two categories: T-fibre fracture dominated or L-fibre fracture dominated.[41,45–47] A T-fibre fracture surface is characterised by the crack plane orients transversely to the fibres and the crack propagates between fibre ends or

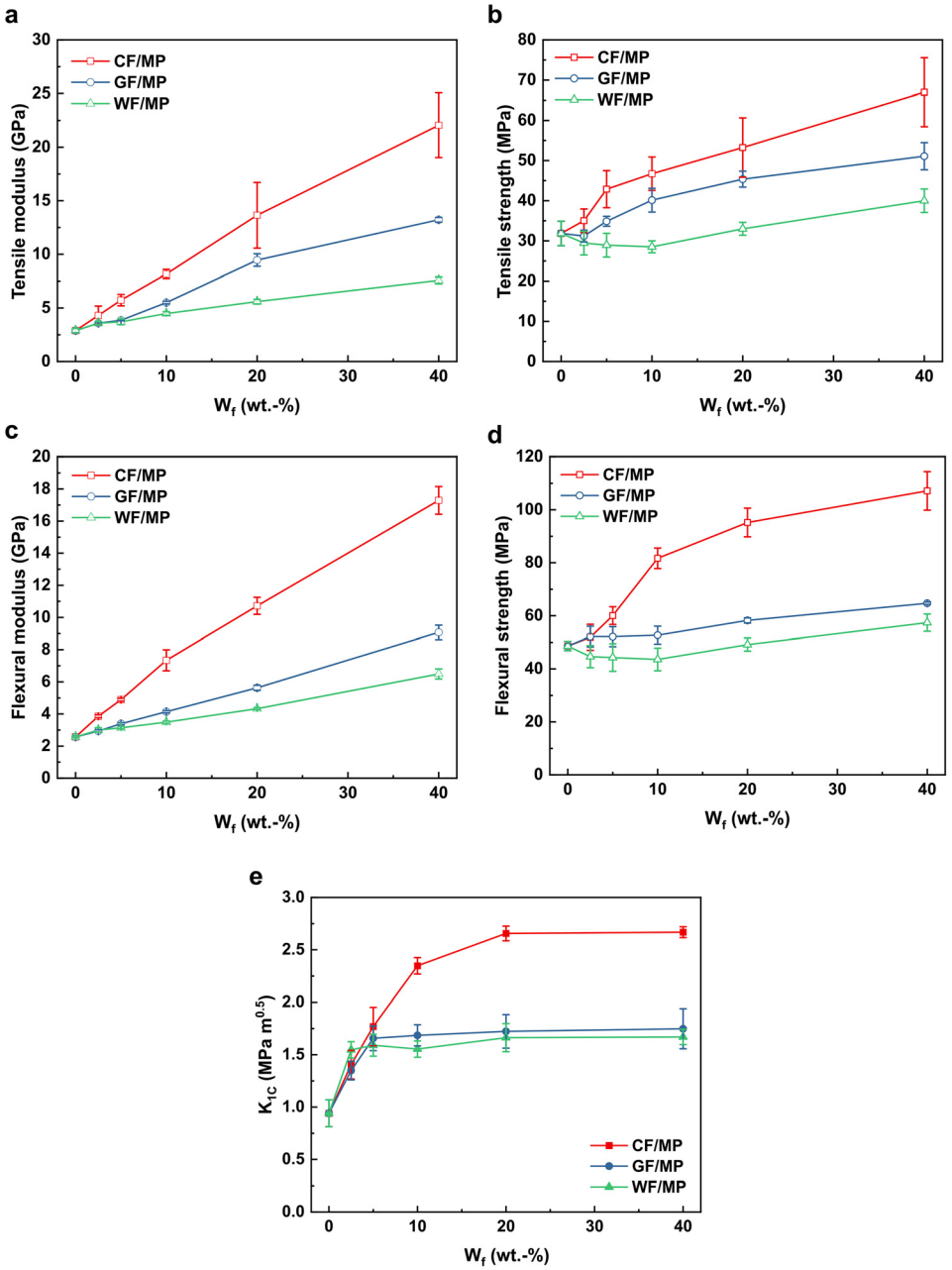

Fig. 6 Mechanical properties of CF-reinforced, GF-reinforced and WF-reinforced industrial mixed plastic. (a) Tensile modulus, (b) tensile strength, (c) flexural modulus, (d) flexural strength, and (e) single-edge notched beam fracture toughness.

broken fibre sites. T-fibre fracture surface exhibits jagged crack profile, crack bifurcations, some fibre breakage, fibre debonding, bridging and pull out, which tend to be associated with high fracture energies associated with the development of new free surfaces on the crack faces. An L-fibre fracture surface is characterised by the fibres orient parallel to the crack plane and is often associated with an area of weakness, such as the mixed plastic matrix. Both GF-reinforced and CF-reinforced mixed plastic show T-fibre fracture dominant. As CFs possess smaller fibre diameter than GFs, higher fracture energy is required, leading to higher K_{IC}.

3.5 LCA of reinforced mixed plastics

The previous sections confirmed our initial hypothesis that the mechanical properties of the reinforced industrial mixed plastics are governed by the fibre or filler reinforcement instead of the more inferior brittle mixed plastic matrix. This will create a stronger demand for industrial mixed plastic that is destined to be sent to landfill and incineration to be re-used in selected engineering applications, potentially reducing the demand for virgin fossil-derived polymers. It should be noted however that the manufacturing of CFs and GFs are energy

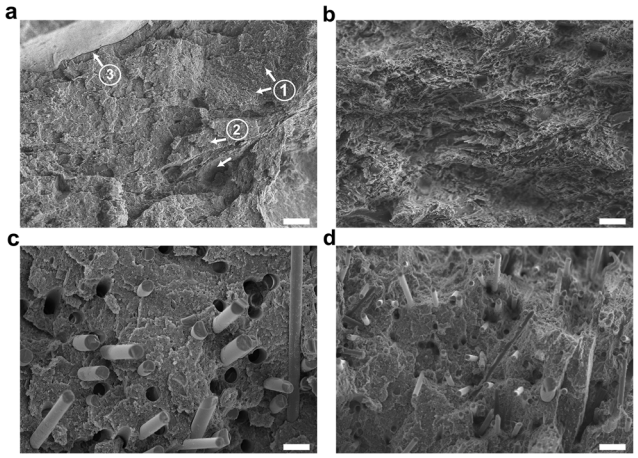

Fig. 7 Fracture surface of (a) unreinforced industrial mixed plastic (b) 20%wt WF-reinforced, (c) 20%wt GF-reinforced and (d) 20% wt CF-reinforced residual mixed plastic (MP). See section 3.4 for label 1–3. Scale bar = 25 μm.

intensive. The energy requirement for the production of polyacrylonitrile (PAN)-based CFs is estimated to be 454 MJ kg^{-1} of CFs.[29] Such high energy requirement stems from the synthesis of PAN (117 MJ kg^{-1}), as well as the stabilisation and carbonisation (150 MJ kg^{-1}) processes. Furthermore, the carbonisation process also produces hydrogen cyanide (HCN) (~0.33 g per metre of CF)[48] as one of the by-products, which are extremely poisonous.[48,49] An energy requirement of 9–22 MJ kg^{-1} is required for the manufacturing of GFs,[50] which stems from the melting and refining of the raw materials (SiO_2, CaO, Al_2O_3, B_2O_3, MgO *etc.*) and the forming processes. The performance upgrade achieved by CFs and GFs reported in Fig. 6 could be offset by the high environmental footprint of CFs and GFs production, making the proposed pragmatic solution an unsustainable one. WF is a more environmentally friendly reinforcing filler and is often used to reduce the cost per unit volume of thermoplastics.[51] However, the mechanical performance improvement was only marginal and there may not be any environmental benefits of reinforcing the brittle mixed plastic matrix with WF. Thus, LCA was conducted.

The mass of a functional unit ($m_{f.u.}$) used in the LCA of sustainable materials reported in the literature is often based on the assumption that the f.u. is a flat plate undergoing either pure elastic deformation under tension[52–55] or bending[24,55,56] only (*i.e.*, $m_{f.u.}$ is calculated from the *specific* tensile or flexural modulus). This significantly underestimates $m_{f.u.}$ as the strength of the material is assumed to be infinitely large. In reality, both the yield strength and ultimate strength need to be considered to ensure that the material used will be able to withstand the expected loads.[57] Here in this work, $m_{f.u.}$ was determined by evaluating the minimum necessary thickness required for the shape of a chair given in Fig. 3 to achieve a global stress state that is the minimum of $\sigma^{Yield}_{Tensile}$, $\sigma^{Yield}_{Flexural}$ or $\sigma_{Fracture}$, whereby $\sigma^{Yield}_{Tensile}$ is the tensile yield strength, $\sigma^{Yield}_{Flexural}$ is the flexural yield strength and $\sigma_{Fracture}$ is fracture strength of the material. The latter term was calculated from the obtained K_{IC} value, assuming the existence of a crack (*e.g.*, fibre inclusion) in an infinite body.[58] Such a design is to ensure that the loads experienced by our f.u. does not exceed the yield strength of the material. An exemplary calculation to determine $m_{f.u.}$ and the $m_{f.u.}$ made from PP and the various (reinforced) mixed plastics can be found in ESI S4.† A comparison of our $m_{f.u.}$ with the $m_{f.u.}$ calculated based on pure elastic deformation under bending is presented in ESI S5.†

Fig. 8 presents the cradle-to-grave global warming potential (GWP) and abiotic depletion potential of fossil fuel (ADPf) of the different lifecycle scenarios. In the case whereby the industrial mixed plastic and our f.u. (a chair made from virgin PP) are sent to landfill and incinerated for energy recovery after use (scenario 1A), was found to contribute to a GWP and a net ADPf of 24 kg CO_2-eq. per f.u. and 431 MJ $f.u.^{-1}$, respectively. The lifecycle scenario whereby all of the industrial mixed plastic from shredder residue was steam gasified (scenario 1B) will still lead to similar GWP, albeit lower net ADPf due to higher energy recovery. The largest contributor in these "business as usual" scenarios is the environmental burden associated with the production and the end-of-life of virgin ABS, PS and PP, accounting for 68% and 22% of the total GWP and ADPf, respectively.

If the industrial mixed plastic from shredder residue was mechanically recycled into our f.u. (scenario 2), LCA showed that the GWP and net ADPf decrease to 14 kg CO_2-eq. per f.u. and 241 MJ $f.u.^{-1}$, respectively. This is because the environmental burden associated with the production of virgin PP for use in the f.u. is avoided, which reduced the GWP by 5.7 kg CO_2-eq. per f.u. and the ADPf by 246 MJ $f.u.^{-1}$. The production of virgin PP not only relies on non-renewable resources, which produce significant environmental burden, but also necessitates the extraction and refinement of petroleum feedstock. These processes involve significant energy inputs (75.5 MJ kg^{-1}).[59] Furthermore, the production of virgin PP entails energy-intensive procedures such as polymerisation, which demands elevated temperatures (reaching up to 230 °C) and pressures (up to 150 bar).[60] These operations also entail the utilization of various chemicals, including catalysts, stabilizers, and solvents.[61]

Scenario 3 presents the lifecycle impact assessment of reinforcing industrial mixed plastic with WF, GFs and CFs. It can be seen that only 40 wt% CF-reinforced mixed plastic possess significantly higher GWP and net ADPf compared to the "business as usual" (scenario 1). When compared to scenario 2 (cascade recycling of industrial mixed plastic) however, all CF-reinforced industrial mixed plastic solutions possess higher GWP and net ADPf, even though these materials possess higher mechanical performance that resulted in lighter f.u. This is because the mechanical performance improvement can no longer offset the environmental burden associated with CF production. GF as reinforcement for industrial mixed plastic is also not an environmental viable solution. At a GF loading <10 wt%, GF-reinforced industrial mixed plastics was found to possess similar GWP and net ADPf as

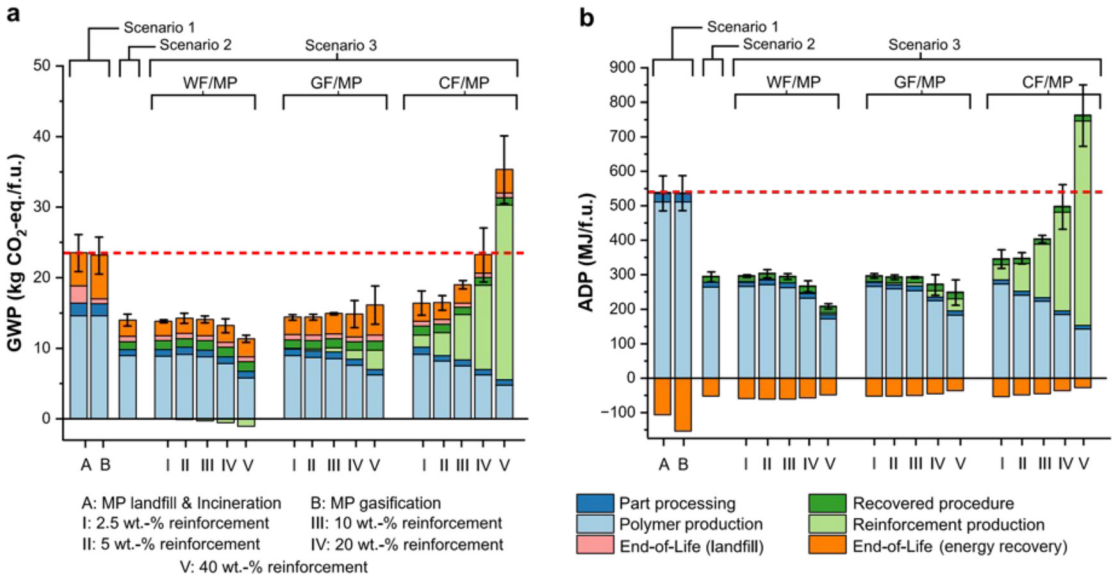

Fig. 8 (a) Global Warming Potential (GWP) and (b) Abiotic Depletion Potential (fossil fuel) (ADPf) of CF-reinforced, GF-reinforced and WF-filled industrial mixed plastic (MP). See section 2.3.6 for the description of each scenario.

unreinforced industrial mixed plastic, implying that the direct mechanical recycling of industrial mixed plastic into the f.u. is the better option. At higher GF loading, the net ADPf was reduced but this was at the expense of GWP as the energy demand increases whilst the fossil demand for the production of polymer matrix decreases with increasing GF loading in the material. Using WF as filler has the advantage of carbon capture during wood growth,[62] resulting in a negative CO_2 emission seen in Fig. 8a. However, the environmental impact of WF-filled industrial mixed plastics at a WF loading of ≤10 wt% was found to be similar to unreinforced mixed plastic. This is due to the poorer mechanical properties of WF-filled mixed plastics. At high WF loading, the environmental impact of WF-filled industrial mixed plastics was lower than unreinforced industrial mixed plastics. This can be attributed to better mechanical performance at higher WF loading (see Fig. 6) as well as a reduction in fossil-derived polymer matrix.

Our LCA model assumes that the end-of-life options for reinforced mixed plastics are landfill and incineration for energy recovery. These are the most likely end-of-life options currently. Nevertheless, our results showed that a composite approach to mechanically upcycle plastic waste is feedstock agnostic. This implies that these reinforced mixed plastics can be recycled as feedstock for new mixed plastic composites, essentially closing the lifecycle loop, achieving circularity potentially. Our hotspot analysis showed that the high environmental burden of GF- and CF-reinforced mixed plastics stemmed from the environmental impact associated with GF and CF productions. Considering that GF composites waste is expecting to grow by 58% to 55 ktonnes per annum and CF composites waste is projected to grow by 160% to 2 ktonnes per year by 2030,[63] this represents an opportunity for our feedstock agnostic mechanical upcycling process. Reclaimed GFs and CFs from end-of-life composites can be used in place of virgin GFs and CFs, further lowering the environmental impact of the resulting mixed plastic composites.

4. Concluding remarks

We demonstrated the feasibility of sustainably upcycling industrial mixed plastic from shredder residue through a composite approach. The extrusion and injection moulding of industrial mixed plastic waste produced a brittle material with poor mechanical properties; E_T of 2.9 GPa, σ_T of 32 MPa, E_f of 2.6 GPa, σ_f of 49 MPa and K_{IC} of 0.94 MPa $m^{0.5}$. This is due to the fact that the different polymers in the industrial mixed plastic are not miscible at a molecular level. Both glass and carbon fibres can effectively reinforce the brittle industrial mixed plastic. The tensile, flexural and fracture toughness properties were found to increase monotonically with increasing GFs and CFs loading. At 40 wt%, CF-reinforced industrial mixed plastic was found to possess E_T of 22 GPa, σ_T of 67 MPa, E_f of 17 GPa, σ_f of 107 MPa and K_{IC} of 2.7 MPa $m^{0.5}$. At the same fibre loading, GF-reinforced industrial mixed plastic possessed E_T of 13 GPa, σ_T of 51 MPa, E_f of 9 GPa, σ_f of 65 MPa and K_{IC} of 1.8 MPa $m^{0.5}$. When WF was used as the reinforcing filler, it was found that both E_T and E_f of the resulting WF-filled industrial mixed plastic waste increased linearly with increasing WF loading up to 7.5 GPa and 6.5 GPa, respectively, but the strength properties exhibited a different trend. Both the σ_T and σ_f decreased initially with increasing WF loading up to 10 wt% before increasing beyond that of unreinforced industrial mixed plastic at higher WF loading up to 40 MPa and 57 MPa, respectively. Our LCA showed that compared to

the "business as usual" scenario, all materials (unreinforced, WF-filled, GF-reinforced and CF-reinforced industrial mixed plastics) with the exception 40 wt% CF-reinforced industrial mixed plastic, have lower environment impact in terms of GWP and net ADPf. Even though GF- and CF-reinforced industrial mixed plastic possessed superior mechanical performance over WF-filled and unreinforced industrial mixed plastic, LCA showed that using GFs and CFs as reinforcements are not the most sustainable option especially when cascade recycling of industrial mixed plastic is employed. This is due to the high environmental burden of producing GF and CF. Whilst counter intuitive, we found that the most sustainable option is to mechanically upcycle industrial mixed plastic with high loading fraction of WF at 40 wt%. This produced not only a material with better mechanical performance than unreinforced industrial mixed plastic but also possess lower environmental burden. Such feedstock agnostic and pragmatic solution of reinforcing industrial mixed plastic at high WF loading has the potential of diverting industrial mixed plastic from landfill and incineration, reducing the demand for fossil-derived virgin polymers and thereby reducing the GWP and net ADPf by 110% and 63%, respectively, compared to "business as usual".

Author contributions

KS: writing – original draft, writing – review & editing, investigation, methodology, conceptualization, data curation. ANG: writing – review & editing, supervision. SRS: writing – review & editing, supervision. KW: writing – review & editing, investigation, data curation. KYL: writing – review & editing, supervision, funding acquisition, conceptualization, project administration, resources.

Conflicts of interest

There are no conflicts to declare.

Acknowledgements

The authors gratefully acknowledge the financial support of the Thailand's National Science and Technology Development Agency, the Office of Educational Affairs for funding KS and Yayasan Khazanah for funding A. N. G. We also greatly appreciate funding provided by the UK Engineering and Physical Science Research Council (EPSRC) for funding this work (EP/S025456/1).

References

1 The Business Research Company, Electrical And Electronics Global Market Report 2022 – By Type (Electrical Equipment, Measuring And Control Instruments, Electronic Products), By End-Use (B2B, B2C), By Sales Channel (OEM, Aftermarket), By Mode (Online, Offline) – Market Size, Trends, And Global Forecast 2022–2026, London, 2022.
2 OICA, Worldwide motor vehicle production growth 2015–2021, https://www.statista.com/statistics/1097267/worldwide-motor-vehicle-production-growth/, (accessed 11 November 2022).
3 Plastics Europe, Plastics-the Facts 2016 An analysis of European plastics production, demand and waste data, 2016.
4 Plastics Europe, Plastics-the Facts 2020 An analysis of European plastics production, demand and waste data, Brussels, 2020.
5 Plastics Europe, Quarterly Report Q1/2022, 2022.
6 O. T. Forton, M. K. Harder and N. R. Moles, *Resour., Conserv. Recycl.*, 2006, **46**, 104–113.
7 F. Passarini, L. Ciacci, A. Santini, I. Vassura and L. Morselli, *J. Cleaner Prod.*, 2012, **23**, 28–36.
8 J. Cui and E. Forssberg, *J. Hazard. Mater.*, 2003, **99**, 243–263.
9 Plastics Europe, *Circular Economy for Plastics – United Kingdom 2020*, Brussels, 2021.
10 D. Mahanta, S. A. Dayanidhi, S. Mohanty and S. K. Nayak, *Polym. Compos.*, 2012, **33**, 2114–2124.
11 B. Chen and J. R. G. Evans, *J. Polym. Sci., Part B: Polym. Phys.*, 2011, **49**, 443–454.
12 J. Gao, X. T. Fu, M. M. Ding and Q. Fu, *Chin. J. Polym. Sci.*, 2010, **28**, 647–656.
13 A. Rudin and N. E. Brathwaite, *Polym. Eng. Sci.*, 1984, **24**, 1312–1318.
14 N. N. Rozik, A. I. Khalaf and A. A. Ward, *Proc. Inst. Mech. Eng., Part L*, 2016, **230**, 526–536.
15 B. L. Rivas and E. D. Pereira, *J. Appl. Polym. Sci.*, 2001, **80**, 2593–2599.
16 J. Maris, S. Bourdon, J. M. Brossard, L. Cauret, L. Fontaine and V. Montembault, *Polym. Degrad. Stab.*, 2018, **147**, 245–266.
17 L. A. Utracki and C. A. Wilkie, *Polymer Blends Handbook*, 2nd edn, 2014.
18 J. Feng, Q. Yuan, X. Sun, F. Yang, K. Cui, W. Li and Z. Yao, *Polym.-Plast. Technol. Mater.*, 2021, **60**, 798–806.
19 A. A. Aziz, H. M. Akil, S. M. S. Jamaludin and N. A. M. Ramli, *Polym.-Plast. Technol. Eng.*, 2011, **50**, 768–775.
20 Y. Wang, Y. Xiao, Q. Zhang, X. L. Gao and Q. Fu, *Polymer*, 2003, **44**, 1469–1480.
21 A. C. Patel, R. B. Brahmbhatt and S. Devi, *J. Appl. Polym. Sci.*, 2003, **88**, 72–78.
22 S. Bonda, S. Mohanty and S. K. Nayak, *Iran. Polym. J.*, 2014, **23**, 415–425.
23 Y. V. Vazquez and S. E. Barbosa, *Waste Manage.*, 2016, **53**, 196–203.
24 A. N. Gaduan, K. Singkronart, C. Bell, E. Tierney, C. Burgstaller and K. Y. Lee, *ACS Appl. Polym. Mater.*, 2021, **4**, 3294–3303.
25 H. Baumann and A.-M. Tillman, *The Hitch Hiker's Guide to LCA- An orientation in LCA methodology and application*, Springer Science and Business Media LLC, 2004, vol. 11.

26 M. Fukushima, M. Shioya, K. Wakai and H. Ibe, *J. Mater. Cycles Waste Manage.*, 2009, **11**, 11–18.
27 A. Vlasopoulos, J. Malinauskaite, A. Żabnieńska-Góra and H. Jouhara, *Energy*, 2023, **277**, 127576.
28 K. Kamijo, H. Tsujimura, H. Obara and M. Katsumata, *SAE Trans.*, 1982, **91**, 2615–2620.
29 F. Meng, J. McKechnie, T. Turner and S. Pickering, *Composites, Part A*, 2017, **100**, 206–214.
30 V. Repellin, A. Govin, M. Rolland and R. Guyonnet, *Biomass Bioenergy*, 2010, **34**, 923–930.
31 L. Ciacci, L. Morselli, F. Passarini, A. Santini and I. Vassura, *Int. J. Life Cycle Assess.*, 2010, **15**, 896–906.
32 M. Larrain, S. Van Passel, G. Thomassen, B. Van Gorp, T. T. Nhu, S. Huysveld, K. M. Van Geem, S. De Meester and P. Billen, *Resour., Conserv. Recycl.*, 2021, **170**, 1–13.
33 J. N. Hahladakis, C. A. Velis, R. Weber, E. Iacovidou and P. Purnell, *J. Hazard. Mater.*, 2018, **344**, 179–199.
34 E. A. Coleman, in *Applied Plastics Engineering Handbook: Processing, Materials, and Applications*, Elsevier Inc., 2nd edn, 2017, pp. 489–500.
35 M. Altarawneh, A. Saeed, M. Al-Harahsheh and B. Z. Dlugogorski, *Prog. Energy Combust. Sci.*, 2019, **70**, 212–259.
36 S. Haveriku, M. Meucci, M. Badalassi, C. Cardelli, G. Ruggeri and A. Pucci, *Micro*, 2021, **1**, 102–119.
37 G. Szarka and B. Iván, *J. Macromol. Sci., Part A: Pure Appl. Chem.*, 2013, **50**, 208–214.
38 Z. O. G. Schyns and M. P. Shaver, *Macromol. Rapid Commun.*, 2021, **42**, 1–27.
39 K. Luo, X. Ye, H. Zhang, J. Liu, Y. Luo, J. Zhu and S. Wu, *Polym. Degrad. Stab.*, 2020, **177**, 109181.
40 A. P. Mathew, S. Packirisamy and S. Thomas, *Polym. Degrad. Stab.*, 2001, **72**, 423–439.
41 E. S. Greenhalgh, in *Failure Analysis and Fractography of Polymer Composites*, ed. E. S. Greenhalgh, Woodhead Publishing, 2009, pp. 279–355.
42 D. Hull and B. T. W. Clyne, *An Introduction to Composite Materials*, Cambridge University Press, 1996.
43 S. Ahmed and F. R. Jones, *J. Mater. Sci.*, 1990, **25**, 4933–4942.
44 B. Dairi, H. Djidjelli, A. Boukerrou, S. Migneault and A. Koubaa, *Polym. Compos.*, 2017, **38**, 1749–1755.
45 A. Sjögren, *Matrix and interface effects on microcracking in polymer composites*, Luleå tekniska universitet, 1997.
46 J. Karger-Kocsis and K. Friedrich, *Compos. Sci. Technol.*, 1988, **32**, 293–325.
47 S. S. Saliba and T. E. Saliba, *Fractography of Modern Engineering Materials: Composites and Metals, Second Volume*, 1993, vol. 2, pp. 23–57.
48 T. Groetsch, M. Maghe, R. Rana, R. Hess, S. Nunna, J. Herron, D. Buckmaster, C. Creighton and R. J. Varley, *Ind. Eng. Chem. Res.*, 2021, **60**, 17379–17389.
49 C. Liu, R. Zhao, Q. Li, R. Yadav, M. R. G. Ferdowsi, Z. Wang, M. An and M. Naebe, *Composites, Part B*, 2023, **255**, 110624.
50 Q. Dai, J. Kelly, J. Sullivan and A. Elgowainy, *Life-Cycle Analysis Update of Glass and Glass Fiber for the GREET Model*, 2015.
51 K. Oksman and C. Clemons, *J. Appl. Polym. Sci.*, 1998, **67**, 1503–1513.
52 M. Hervy, S. Evangelisti, P. Lettieri and K. Y. Lee, *Compos. Sci. Technol.*, 2015, **118**, 154–162.
53 T. Corbière-Nicollier, B. Gfeller Laban, L. Lundquist, Y. Leterrier, J.-A. E. Månson and O. Jolliet, *Resour., Conserv. Recycl.*, 2001, **33**, 267–287.
54 M. Pietrini, L. Roes, M. K. Patel and E. Chiellini, *Biomacromolecules*, 2007, **8**, 2210–2218.
55 J. R. Duflou, D. Yelin, K. Van Acker and W. Dewulf, *CIRP Ann. - Manuf. Technol.*, 2014, **63**, 45–48.
56 A. Le Duigou and C. Baley, *J. Cleaner Prod.*, 2014, **83**, 61–69.
57 M. F. Ashby, in *Materials Selection in Mechanical Design*, ed. M. F. Ashby, Butterworth-Heinemann, Oxford, 4th edn, 2011, pp. 57–96.
58 H. T. Corten, *Fracture Toughness: Part II*, American Society for Testing & Materials, Philadelphia, 1972.
59 F. Associates, *Cradle-to-gate life cycle analysis of Polypropylene (PP) resin- Final report*, 2021.
60 A. Alsabri, F. Tahir and S. G. Al-Ghamdi, *Polymer*, 2021, **13**, 3793.
61 C. Paulik, C. Tranninger, J. Wang, P. Shutov, D. Mileva and M. Gahleitner, *Macromol. Chem. Phys.*, 2021, **222**, 2100302.
62 A. Mishra, F. Humpenöder, G. Churkina, C. P. O. Reyer, F. Beier, B. L. Bodirsky, H. J. Schellnhuber, H. Lotze-Campen and A. Popp, *Nat. Commun.*, 2022, **13**, 4889.
63 V. Sommer, J. Stockschläder and G. Walther, *Waste Manage.*, 2020, **115**, 83–94.
64 A. N. Gaduan, J. Li, G. Hill, C. Wallis, C. Burgstaller and K.-Y. Lee, *Resour., Conserv. Recycl.*, 2023, **189**, 106734.

